Bioactive Materials 8 (2022) 296–308

Contents lists available at ScienceDirect

Bioactive Materials

journal homepage: www.sciencedirect.com/journal/bioactive-materials

In vivo printing of growth factor-eluting adhesive scaffolds improves wound healing

Kristo Nuutila [a,1,***], Mohamadmahdi Samandari [b,1], Yori Endo [a], Yuteng Zhang [a], Jacob Quint [b,c], Tannin A. Schmidt [b], Ali Tamayol [b,c,**], Indranil Sinha [a,*]

[a] Division of Plastic Surgery, Brigham and Women's Hospital, Harvard Medical School, Boston, MA, 02115, USA
[b] Department of Biomedical Engineering, University of Connecticut, Farmington, CT, 06030, USA
[c] Department of Mechanical and Materials Engineering, University of Nebraska-Lincoln, Lincoln, NE, 68588, USA

ARTICLE INFO

Keywords:
In vivo printing
Handheld bioprinter
Adhesive scaffolds
GelMA
VEGF
Wound healing

ABSTRACT

Acute and chronic wounds affect millions of people around the world, imposing a growing financial burden on patients and hospitals. Despite the application of current wound management strategies, the physiological healing process is disrupted in many cases, resulting in impaired wound healing. Therefore, more efficient and easy-to-use treatment modalities are needed. In this study, we demonstrate the benefit of *in vivo* printed, growth factor-eluting adhesive scaffolds for the treatment of full-thickness wounds in a porcine model. A custom-made handheld printer is implemented to finely print gelatin-methacryloyl (GelMA) hydrogel containing vascular endothelial growth factor (VEGF) into the wounds. *In vitro* and *in vivo* results show that the *in situ* GelMA crosslinking induces a strong scaffold adhesion and enables printing on curved surfaces of wet tissues, without the need for any sutures. The scaffold is further shown to offer a sustained release of VEGF, enhancing the migration of endothelial cells *in vitro*. Histological analyses demonstrate that the administration of the VEGF-eluting GelMA scaffolds that remain adherent to the wound bed significantly improves the quality of healing in porcine wounds. The introduced *in vivo* printing strategy for wound healing applications is translational and convenient to use in any place, such as an operating room, and does not require expensive bioprinters or imaging modalities.

1. Introduction

Skin integrity is instrumental to protect the body from the external environment, regulate body temperature, and prevent dehydration [1]. Therefore, the ability of the body to ensure skin integrity, by healing wounds, is an essential physiological process. Wound healing consists of three overlapping phases: inflammation, proliferation, and remodeling [2,3]. However, wounds may, pathologically, fail to progress through the normal healing pathway [4]. These wounds either under-heal and become chronic or over-heal and form excess fibrous connective tissue that results in scarring [5,6]. Despite the utilization of current wound treatments, compromised wound healing affects nearly 8 million people in the United States annually, and incur staggering healthcare costs [7]. Novel and more efficient treatment modalities are needed to treat patients with poorly healing wounds [8].

While autografts are considered the "gold standard" approach for the treatment of severe skin injuries, their application is limited by variable tissue integration, incomplete functional recovery, and donor site morbidity [9]. Recent developments in tissue engineering and drug delivery technologies have presented promising alternative approaches, either alone or combined with traditional wound treatments [10–13]. Different scaffolding biomaterials, such as hydrogels, have been implemented as artificial grafts to improve wound closure [9,10]. Hydrogels are interesting candidates as dermal substitutes, due to their similarity to native extracellular matrix, tunable mechanical and chemical properties, and their cell permissibility [14–17]. Furthermore, many studies

Peer review under responsibility of KeAi Communications Co., Ltd.
* Corresponding author. Division of Plastic Surgery, Brigham and Women's Hospital, Harvard Medical School, Boston, MA, 02115, USA.
** Corresponding author. Department of Biomedical Engineering, University of Connecticut Health Center, Farmington, CT, 06030, USA.
*** Corresponding author. Division of Plastic Surgery, Brigham and Women's Hospital, Harvard Medical School, Boston, MA, 02115, USA.
E-mail addresses: kristo.nuutila@gmail.com (K. Nuutila), atamayol@uchc.edu (A. Tamayol), isinha@bwh.harvard.edu (I. Sinha).
[1] K. Nuutila and M. Samandari contributed equally to the work.

https://doi.org/10.1016/j.bioactmat.2021.06.030
Received 14 April 2021; Received in revised form 16 June 2021; Accepted 24 June 2021
Available online 5 July 2021

suggest that the application of hydrogels, with controlled release of bioactive factors, using active or passive delivery strategies, can improve wound healing [18,19]. Controlled, local release of drugs from hydrogels can boost the healing process while preventing a systemic drug toxicity [20,21].

Injectable hydrogels with *in situ* gelation and prefabricated hydrogel grafts demonstrated promising outcomes for tissue regeneration [22]. However, these scaffolds suffer from poor tissue integration specifically when dealing with open wounds, due to the irregular shape of the defect and limited scaffold fidelity or adhesion, which necessitates fixation modalities. Creating hydrogel grafts with complex geometry and proper structural stability into open defects on curved surfaces requires an accurate control on the deposition and crosslinking of the bioink. 3D bioprinting has been implemented for the fabrication of more complex scaffolds to be implanted into the wound site [23,24]. While bioprinting strategies can indeed offer an automated fabrication of complex scaffolds, they have several drawbacks. First, these systems require highly complicated expensive facilities for imaging the defects, analyzing its shape and size, and printing the corresponding scaffold [25]. Moreover, the 3D printed hydrogel scaffolds are not typically adhesive [26]. This necessitates the implementation of fixation modalities. Even still, the non-adherent scaffolds are susceptible to detach during motion, which will impair their tissue integration. In addition, most currently available stationary bioprinters are unable to print scaffolds on curved surfaces [25,27,28].

Recently, there has been a new trend in directly printing scaffolding materials into the defect site [25]. *In situ* bioprinting minimizes the preparation time of scaffolds, promotes rapid wound closure, and limits fibrosis [29–31]. Two main *in situ* bioprinting strategies have been developed in regenerative medicine: robotic *in situ* printing [31] and handheld *in situ* printing [32]. Although *in situ* printing using a robotic system can be highly accurate and reliable, it requires complex and expensive facilities, imaging tools, and computer-aided techniques for analysis and reconstruction of defects with irregular shapes. Recently developed, handheld bioprinters minimize the complexity of *in situ* printing by eliminating the requirement of imaging modalities, while allowing the printing of irregular shape scaffolds on curved surfaces [32–37]. Using this strategy, the defect structure can be inspected and scaffolding material can directly be deposited into the wound, conforming to any shape or topography. In a prominent study, a handheld printer was developed that could deposit hydrogel strips onto the wound surface [32,38]. A two-barrel handheld extruder was used to simultaneously extrude scaffolding material and its crosslinker through a microfluidic printing head. While the printing of wide hydrogel strips allows for rapid wound coverage, it is challenging to conform to irregular shapes and crevices. Furthermore, the need for application of a crosslinking reagent can make the *in situ* printing more challenging and less biocompatible. A special attention therefore is required to be devoted for the selection of bioink for *in situ* printing in wound healing applications. In addition to printability and biocompatibility, the bioink needs to establish a strong adhesion upon crosslinking. This prevents the detachment of the graft due to the body movement and allows rapid tissue engraftment [33]. Additionally, bioinks can be supplemented with regenerative factors, specifically to regulate impaired physiological processes post major injuries [39,40].

In this study, a custom-made and easy-to-use handheld bioprinter is utilized to apply gelatin-methacryloyl (GelMA) hydrogel containing vascular endothelial growth factor (VEGF) to promote tissue regeneration and improve wound healing. The application of fine nozzle in the handheld bioprinter enables accurate filling of defects with irregular shapes while the capability of tuning the flow rate in a wide range provides the control over the speed of printing for small and large size wounds. GelMA was selected to address the mentioned requirements of printability, biocompatibility, and mechanical properties. It further allows the sustained release of encapsulated molecules, such as growth factors, following photocrosslinking. Given the importance of proper vascularization for improved wound healing [41], VEGF was selected as the therapeutic factor loaded into the GelMA scaffold. VEGF can enhance the activity of endothelial cells and induces angiogenesis [4]. The proper vascularization can ensure sufficient tissue oxygenation and metabolic support, and a regulated physiological responses to the dynamic wound environment [41]. While VEGF-loaded biomaterials have been previously utilized to improve wound healing [42,43], the aim of this study is to develop and evaluate the translational feasibility of an *in vivo* printing strategy, for timely treatment of wounds with a VEGF-loaded bioink. In the first phase of this study, the properties of VEGF containing GelMA hydrogels and its influence on the behavior of endothelial cells were studied and optimized *in vitro*. Subsequently, in the second phase, the effect of *in vivo* printing of this scaffold on the healing and its translational feasibility were investigated in a full-thickness porcine wound healing model.

2. Results and discussion

2.1. A custom-made handheld bioprinter enables in situ printing

Handheld bioprinters provide an opportunity for direct printing of a scaffold onto a wound surface. In this study, we used *in situ* printing of VEGF-releasing scaffolds to improve wound healing (schematic in Fig. 1A). A custom-made, partially-automated handheld bioprinter was fabricated, with an embedded ultraviolet (UV) light, which enables *in situ* crosslinking of the photo-polymerizable bioinks (Fig. 1B). The printer utilizes an extrusion system based on the transfer of rotational motion of an electric motor into linear motion, pushing the plunger of a syringe carrying the bioink. The device enables a stable plunger motion with a variability less than 5% of the set value. The handheld printer is able to quickly and easily print filaments into any shape (Fig. 1C). The deposition rate of the device could be controlled in a wide range of 4 μL/s to 18 μL/s, suitable for treatment of small and large defects (Fig. 1D). A lower flowrate improves the control over the shape and architecture of the deposited scaffold, while the higher flowrate allows rapid printing for timely covering of the large wound surfaces. Furthermore, the resolution of the bioprinting could be controlled by tuning the diameter of deposited filament below the millimeter scales through changing the traveling speed of the printing (Fig. 1E; details are provided in the Experimental Section). It can be seen that the diameter of the filament reduced by increasing the moving speed (hand movement speed) at a constant extrusion rate.

The *in situ* printing strategy significantly promotes the flexibility of the treatment by allowing the scaffolds deposition onto irregular-shaped defects, on the curved surfaces, and even on moving body parts. *In situ* crosslinking can potentially result in the enhanced adhesion of the scaffold, minimizing the requirement of fixation modalities for the implanted scaffold [33]. The adhesion of the scaffold to the native remnant tissue is an important feature considering the challenges of implanting *in vitro* fabricated soft scaffolds into the defect [33,44]. It should be noted that the integrated light used for *in situ* crosslinking is a 395 nm wavelength light, at the border of UV-A and visible light spectrums, which have been widely used in the medical applications for biopolymer crosslinking. It has been previously shown that exposure to such low intensity light for short periods of time has negligible detrimental effect on cellular behavior, even at lower ranges of wavelengths in UV-A spectrum [45–47].

While the repeatability of handheld devices is expected to be lower than conventional automated 3D printers, they offer sufficient resolution to allow precise filling of the defects in tissues with irregular shapes such as injured skin. Implementing this device, we demonstrated successful *in vivo* printing of growth factor loaded GelMA within the wound site.

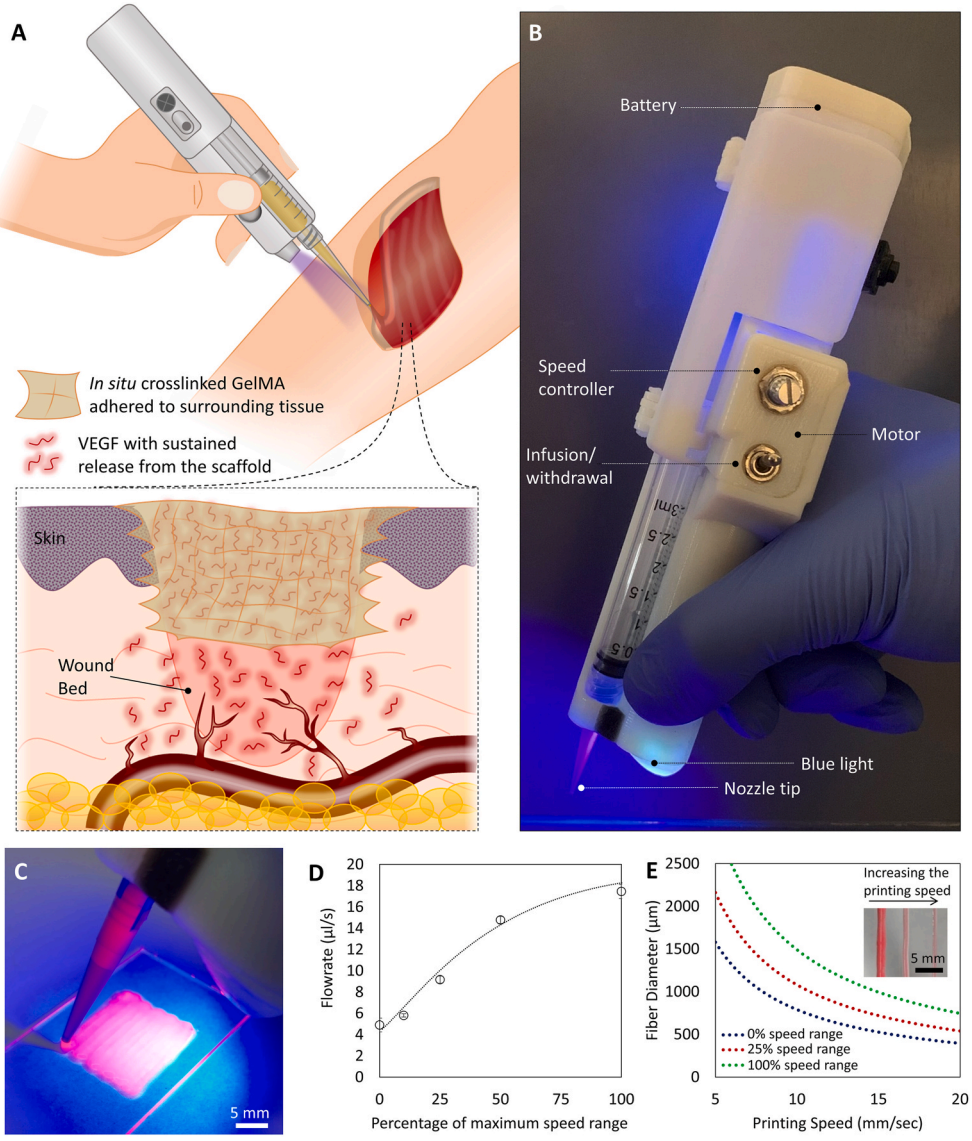

Fig. 1. *In vivo* printing of growth factor-eluting hydrogel for wound healing applications. (A) Schematic representation of the *in vivo* printing strategy. GelMA precursor supplemented with VEGF is extruded using a handheld printer and photo-crosslinked *in situ*. This approach enables the treatment of a wound with irregular shapes and on curved surfaces. *In situ* crosslinking offers the adhesion of the scaffold to the tissue and eliminates the requirement of fixation modalities. The released VEGF promotes angiogenesis in the wound bed and consequently enhances the quality and rate of wound healing. (B) The portable handheld printer used in this study. The device is a partially automated system allowing the adjustment of deposition rate and *in situ* photo-crosslinking with an integrated UV light. (C) Printing of hydrogel scaffolds for precise deposition of the bioink using the handheld printer. (D) The deposition rate of the device can be adjusted in a continuous manner, in the range of 4 µL/s to 18 µL/s (n = 4 was used for each point). (E) The diameter of the deposited filaments can be adjusted based on the printing speed and the applied flow rate. Inset shows the hydrogel filaments printed with different sizes. Here, a 22-gauge tapered nozzle was used.

2.2. Characterization of GelMA ink for in situ printing

An ideal bioink should be printable, supportive for cellular ingrowth, biodegradable, and allow for cell attachment [47,48]. The bioink must offer a suitable viscosity to enable controllable printing with excellent shape fidelity [49]. In addition, the mechanical properties of the crosslinked scaffold need to be tuned for regeneration applications [50]. Specifically for wound healing applications, a soft scaffold, similar to a temporary fibrin network, is preferred [51]. Softer gels, which are easier to be remodeled by nascent cells, better support cell infiltration and spreading [52,53].

GelMA is reported to serve as a suitable scaffolding hydrogel due to the similarity of its structure to native ECM, the presence of cell attachment sites and degradable sequences in its structure, easy photocrosslinking, and controllability over its mechanical properties [45,47,54,55]. Therefore, GelMA was selected in this study and its concentration was optimized to offer decent printability, suitable tissue adhesion, and support cellular function (Fig. 2). Fig. 2A shows the results of the mechanical properties evaluation based on a compression test. The scaffolds were being printed at the stretched state of the native tissue where tissue movements are expected to compress the scaffolds. Therefore, the mechanical properties of the hydrogels were measured in response to compressive loads. Three different concentrations were evaluated: 6%, 9% and 12% (w/v). A compression modulus of 1.2 ± 0.2 kPa (mean ± SD), 4.1 ± 0.2 kPa, and 10.6 ± 0.8 kPa was observed for 6%, 9% and 12% (w/v) GelMA scaffolds, respectively. We also evaluated the adhesion strength of *in situ* crosslinked GelMA to porcine skin. Using a setup depicted in Fig. 2B, the shear adhesion strength of the printed hydrogel to porcine skin was assessed. An adhesion strength of 3.7 ± 1, 6.3 ± 0.5 and 10.3 ± 2.5 kPa was obtained for 6%, 9%, and 12% GelMA, respectively. These adhesion strengths are close to the shear strength of the material itself, as demonstrated by the failure of most samples in the bulk GelMA rather than the adhesion interface with the skin (Fig. 2C). Scanning electron microscopy (SEM) evaluations further confirmed good binding between the GelMA and skin microstructures (Fig. 2D).

GelMA has been implemented as a bioadhesive for regenerative applications [56,57]. The strong GelMA-tissue adhesion upon *in situ* crosslinking is attributed to physical interlocking, the generation of free radicals during photocrosslinking that forms covalent bonds, and hydrogen bonds formed due to the presence of free hydroxyl groups in the hydrogel structure [57,58]. As demonstrated by our results (Fig. 2B and C), the adhesion strength of the *in situ* crosslinked GelMA is close to the shear strength of the material, and therefore can be modulated with hydrogel concentration. Through manipulation of the GelMA

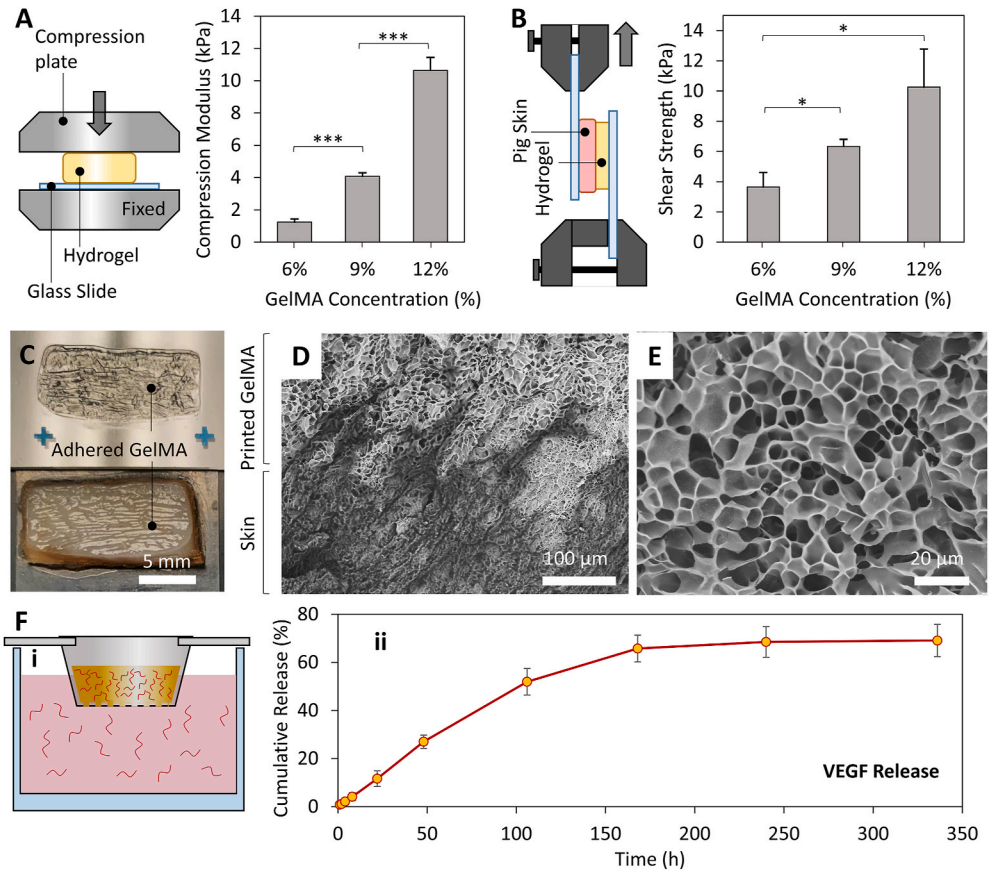

Fig. 2. Characterization of the printing bioink for wound healing application. (A) Evaluating the elastic modulus of GelMA hydrogel with different concentrations through compression tests. While a softer hydrogel is preferred for enhanced cell spreading and migration, 9% GelMA was selected as the bioink formulation in this study due to the limited printability of material having lower concentrations. (B) The assessment of the *in situ* crosslinked GelMA adhesion strength to skin using a modified shear test. The setup used for shear tests is schematically shown. (C) A representative sample from the shear tests demonstrating that the failure occurred from the bulk GelMA rather than adhesion interface with the skin. (D) SEM cross-section micrograph of the GelMA/pig skin interface demonstrating a proper binding between two microstructures. GelMA is the top brighter region in the image while the pig skin is the darker bottom area. (E) A magnified SEM micrograph showing the internal porous structure of GelMA hydrogel. (F) Release assessment studies demonstrating the capability of the hydrogel network to offer a sustained release of VEGF molecules. The setup used in this study is shown in (i), while the VEGF release profile is shown in (ii). n = 6 in mechanical properties evaluation and n = 4 for release experiments were utilized.

concentration and crosslinking time, previous studies have demonstrated that the adhesion strength could be tuned to be comparable to that of commercially available tissue adhesives but with superior biocompatibility and cell permissibility [56,57]. In this study, GelMA is implemented as a temporary scaffold releasing angiogenic factors for improved wound healing. Therefore, a softer hydrogel with higher cell permissibility is preferred, while the adhesion properties close to the material strength is enough for our *in vivo* printing and subsequent tissue integration.

For *in situ* printing using our device, the pre-warmed bioink at 37 °C was first loaded into the syringe followed by its incubation at room temperature for 5–10 min to allow its partial gelation as a result of temperature reduction [53]. The partial gelation increases the viscosity of the bioink and allows easy deposition using the handheld device. However, due to the low concentration of 6% GelMA in our study, its printability and final shape fidelity were inadequate for *in situ* printing applications. Higher concentrations of the GelMA (9% and 12%) were further examined (Fig. S1), and the 9% solution was selected to be used in the animal study due to its better printability and lower stiffness. As mentioned before, lower stiffness is expected to expedite cell infiltration and spreading inside the GelMA scaffolds [54].

The internal microstructure of applied GelMA in this study was further evaluated using SEM (Fig. 2E). A porous hydrogel structure, with an average pore size of 9.57 µm was detected using the SEM analysis of the lyophilized hydrogel. While the SEM analysis upon lyophilization is widely used for evaluating the internal microstructure of the GelMA [45], critical point drying was also performed to further confirm the porous microstructure of the implemented GelMA hydrogel, not affected by the freeze-drying step (Fig. S2). Such porous structures can help cell spreading and migration, and enables the rapid transport of nutrients, oxygen, and wastes through the structure, all necessary for proper regeneration [16]. The porous nature of the scaffolds further enables the sustained release of therapeutics [40,59]. The results of our release studies demonstrated the capability of the structure to preserve VEGF molecules and release them over time (Fig. 2F). The cumulative release profile demonstrate that a gradual long-term release can be obtained up to several days. This significantly enhances the local availability of the therapeutics in the wound environment.

It is also important that the released VEGF from the hydrogel remains intact over time in a physiological temperature. To ensure the integrity of the growth factor released from the GelMA, western blot analysis was performed on the samples collected at day 7 of the release study. The results demonstrated that the majority of the released VEGF remains intact, with an apparent molecular weight close to 30 kDa, similar to the reported value by the provider (Fig. S3).

2.3. Released VEGF promotes endothelial cell migration in vitro

Proper vascularization of the wound bed, ensures sufficient metabolic support throughout the healing process, the proper immune response to potential infection, and a balanced infiltration of the cells associated with regeneration [3]. Sustained release of VEGF is used in this study for the stimulation of the endothelial cells and induction of angiogenesis. To ensure the effectiveness of the released VEGF from the printed scaffold on enhancing the migration of endothelial cells, prior to animal studies, a standard *in vitro* scratch assay [40] was carried out (Fig. 3). A confluent monolayer of human umbilical vein endothelial cells (HUVECs) was scratched and then treated with VEGF released from GelMA to evaluate its effect on cell migration (Fig. 3A). Four different groups underwent the scratch assay: (i) a negative control group, in which the scratch did not receive any treatment, (ii) a blank GelMA group, (iii) a VEGF-eluting GelMA group, and (iv) a positive control group treated directly with VEGF. Fig. 3B and C demonstrate the qualitative and quantitative outcomes. Over time, the cells, which were

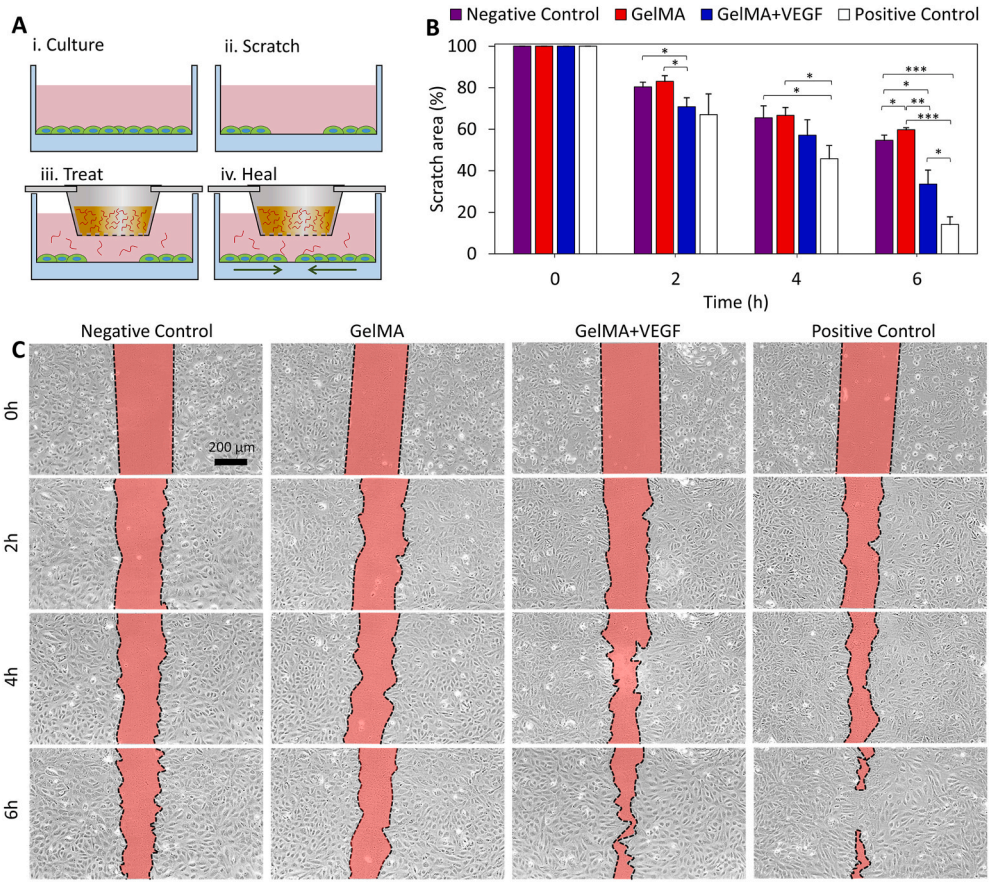

Fig. 3. The effect of VEGF released from the GelMA network on the functionality of HUVECs. (A) A scratch assay was designed to examine the effectiveness of the release strategy on the migration of endothelial cells. Following the formation of a confluent monolayer of HUVECs, a scratch was made and treated with different conditions placed into cell culture media. (B) Quantitative assessment of the scratch assay results. Four different groups were compared to understand the effect of GelMA releasing VEGF on the activity of endothelial cells. The results confirm the beneficial effect of strategy for enhancing cellular activity. n = 3 was used at each time-point. (C) Representative images of the scratch area over time.

confluent in the vicinity of the gap, migrate to the available space generated by the scratch. The comparison between the positive and negative control groups confirmed that the migration capability of the HUVECs can be improved by supplementation of VEGF. Furthermore, by comparing the GelMA + VEGF group with the GelMA and negative control, it is demonstrated that GelMA alone did not have a positive effect on cell migration while the released VEGF from the GelMA network in the GelMA + VEGF group could significantly enhance the migration of HUVECs. These data suggest that the encapsulated VEGF remained functional throughout the scaffold fabrication process.

2.4. *In vivo printing of VEGF-eluting GelMA scaffolds improves wound healing in a porcine model*

In order to evaluate the translational feasibility of the *in vivo* printing strategy and its efficacy for wound healing applications, porcine full-thickness wound model was implemented in this study. Fig. S4 indicates the workflow of the animal studies in this work. Circular dorsal wounds were created and the borders of the wounds were tattooed. The wounds were randomly divided into four different treatment groups: i) no treatment (as a negative control), ii) topical VEGF delivery, iii) *in situ* printed, blank GelMA scaffolds, and iv) *in situ* printed GelMA scaffolds supplemented with VEGF. We implemented a previously verified VEGF dosage required for induction of vascularization, and consequent improvement in wound healing, in small and large animals (see Experimental Section for more details) [4,60]. Additionally, the optimized concentration of GelMA (9%) was used for the treatments and printing was performed at 5 μL/s. Wound healing was evaluated at 7 and 14 days post injury. All of the printed hydrogels were adhered to the surrounding tissue after printing and during wound inspections throughout the study.

2.4.1. *Macroscopic evaluation of wound healing*

Macroscopic wound closure was evaluated on days 7 and 14 (Fig. 4). Representative photographs (Fig. 4A) and the quantitative results (Fig. 4B–D) showed that the wounds in all groups had closed relatively well, which can be due to the use of healthy young pigs in the study. The analysis showed that by day 7, the wounds were more than 60% smaller in comparison to the original wound area. On day 14 post-surgery, the remaining wounds were similarly closed compared to the original size in all groups. Although no statistically significant differences were observed in the macroscopic wound closure, a significant difference was observed in the wound healing mechanism. Similar to humans, porcine wounds normally heal by formation of granulation tissue and re-epithelialization, as well as contraction [61,62].

Wound contraction was measured from the macroscopic photos using the tattooed wound margins (Fig. 4B). The results showed that by day 14, the wounds treated with the bioprinted GelMA containing VEGF had minimally contracted (18 ± 4%), which was significantly less than blank GelMA (30 ± 2%), Topical VEGF (31 ± 4%) and control groups (46 ± 3%) (Fig. 4E). Blank GelMA treated also exhibit significantly less contraction than non-treated wounds. While contraction is a reparative mechanism following full-thickness skin injury, excessive contraction can lead to hypertrophic scarring, poor cosmetic outcomes, and limit the functionality of the healed tissue [5,63]. Furthermore, the mechanical properties of the contracted scarred skin is typically weaker than the original tissue, increasing the possibility of wound reopening [64]. As such, novel therapeutics aim to limit the contracture rate [65]. Commercially available dermal regenerative matrixes and cellulose hydrogels have shown to modestly decrease wound contracture rate and promote functional recovery following wound creation, but these systems require cutting and suturing to conform to wound edges [66]. These matrixes should also be secured in place by suturing.

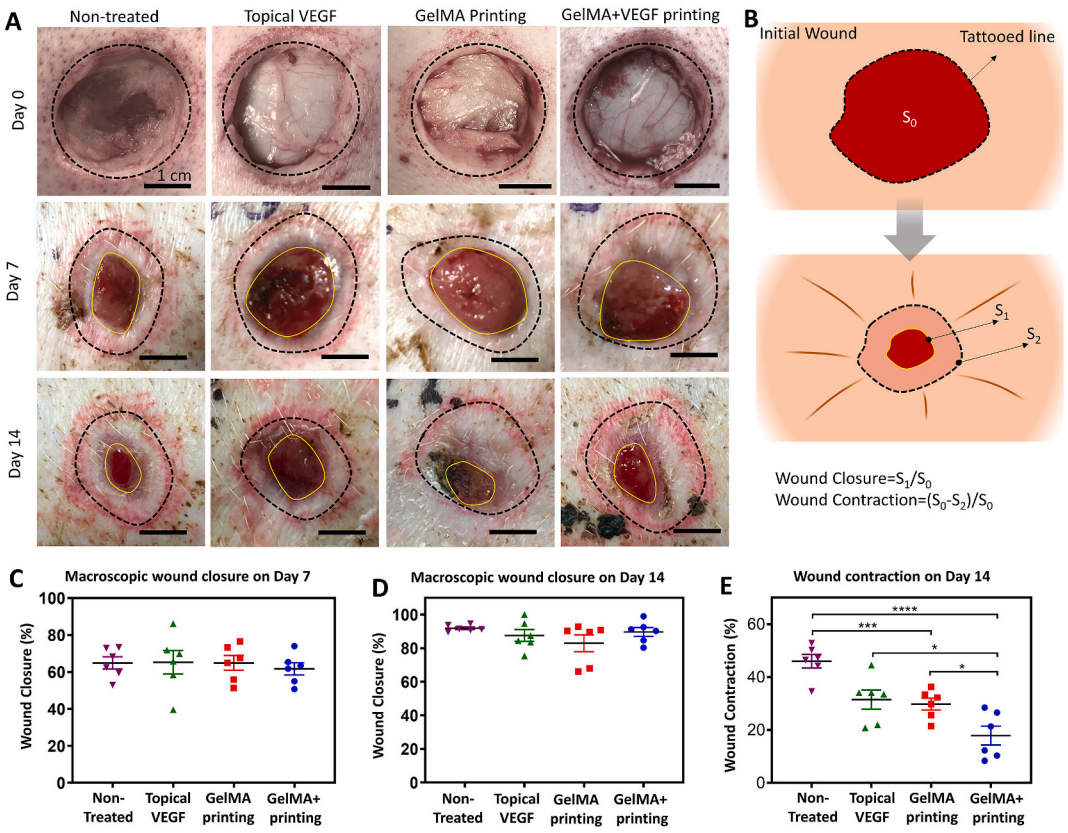

Fig. 4. Macroscopic wound closure. (A) Representative pictures of the wounds administrated with different treatments on day 7 and day 14 post surgery. (B) Schematic illustration of the method for quantification of wound closure and contraction. Quantitative evaluation of macroscopic wound closure on (C) day 7 and (D) day 14 post surgery. (E) Wound contraction relative to the original wound size. While no statistically significant difference was observed in macroscopic wound closure, the wounds treated by *in vivo* printing of GelMA releasing VEGF had contracted significantly less than the other groups. In addition, the blank GelMA treated wounds exhibit significantly less contraction than the non-treated wounds. n = 6 used for all quantifications.

2.4.2. *Microscopic evaluation of wound healing*

Microscopic analysis of wound healing further supported a significant improvement in the wound healing quality following *in vivo* printing of VEGF-eluting GelMA scaffold. Fig. 5 includes representative pictures of the wound bed stained with hematoxylin and eosin (H&E, Fig. 5A–C), and their quantitative characterization (Fig. 5D–I). A higher level of wound re-epithelialization and granulation tissue was observed as a result of *in vivo* printing of VEGF-eluting GelMA scaffolds compared to the other groups, though, most of the wounds were relatively well re-epithelialized and granulated after 14 days, in all groups (Fig. 5D, F).

The ratio of total scar connective tissue area to the area of underlying dermis was measured to obtain scar elevation index (SEI) of each wound (SEI=(S1+S2)/S1 shown in Fig. S5) [67]. A SEI of 1 is indicative of minimal scarring, while a higher number represents pathologically increased scarring. In accordance to the macroscopic wound healing results, the SEI was significantly less in the wounds treated with *in situ* printing of VEGF-eluting GelMA (Fig. 5F). The SEI in the wounds treated with VEGF-eluting GelMA was (1.09 ± 0.01), which was significantly less than the amount after treatment with blank GelMA (1.21 ± 0.05), topical VEGF treatment (1.24 ± 0.02), and non-treated wounds (1.31 ± 0.06).

The regenerated epithelium was further evaluated by quantifying epidermal thickness and number of rete ridges. Thickness of the neo-epidermis in the wounds treated with VEGF-eluting GelMA scaffolds (165 ± 28 μm) was significantly increased in comparison to the blank GelMA (130 ± 14 μm), topical VEGF (95 ± 13 μm), and non-treated wounds (85 ± 7 μm) (Fig. 5B and G). A similar trend was observed in the number of rete ridges in the neoepidermis. The number of rete ridges in the VEGF-eluting GelMA (9.32 ± 1.37) was higher compared to the wounds treated with blank GelMA (4.54 ± 1.16), topical VEGF (6.86 ± 0.52), and non-treated wounds (4.69 ± 0.98). The differences between the VEGF-eluting GelMA, topical VEGF, and non-treated wounds were statistically significant (Fig. 5B and H). Similarly, other studies have shown an optimal wound environment results in thicker epidermis and denser rete ridge formation [68,69].

Finally, the degree of inflammation was studied by analyzing the H&E stained wound sections for infiltration of inflammatory cells to the wound bed. The results demonstrated that while inflammation was present in all wounds, the VEGF-eluting GelMA treated wounds contained the fewest number of inflammatory cells. The differences between the GelMA with VEGF and the VEGF in PBS and non-treated wounds were statistically significant (Fig. 5C and I). Previous studies suggested that an optimal wound healing environment results in less inflammation, which is consistent with the present study [70,71].

It has been reported that VEGF is important for skin wound healing, playing a key role in collagen deposition, angiogenesis, granulation tissue formation and epithelization [72], our results demonstrate that topical and abrupt administration of VEGF alone does not significantly improve the re-epithelialization and granulation. This finding aligns with pertinent literature suggesting the importance of VEGF bioavailability throughout the wound healing [4,21]. The concentration of VEGF delivered through a burst release in the wound bed can be quickly decreased due to high fluid turnover in the wound area, considering the low penetration rate of VEGF topically administered [4,21].

Quality of healing analyses demonstrated that the *in vivo* printing of GelMA containing VEGF treatment resulted in better skin regeneration after wounding. The results showed that wound contraction and degree of hypertrophy were significantly reduced in the GelMA containing

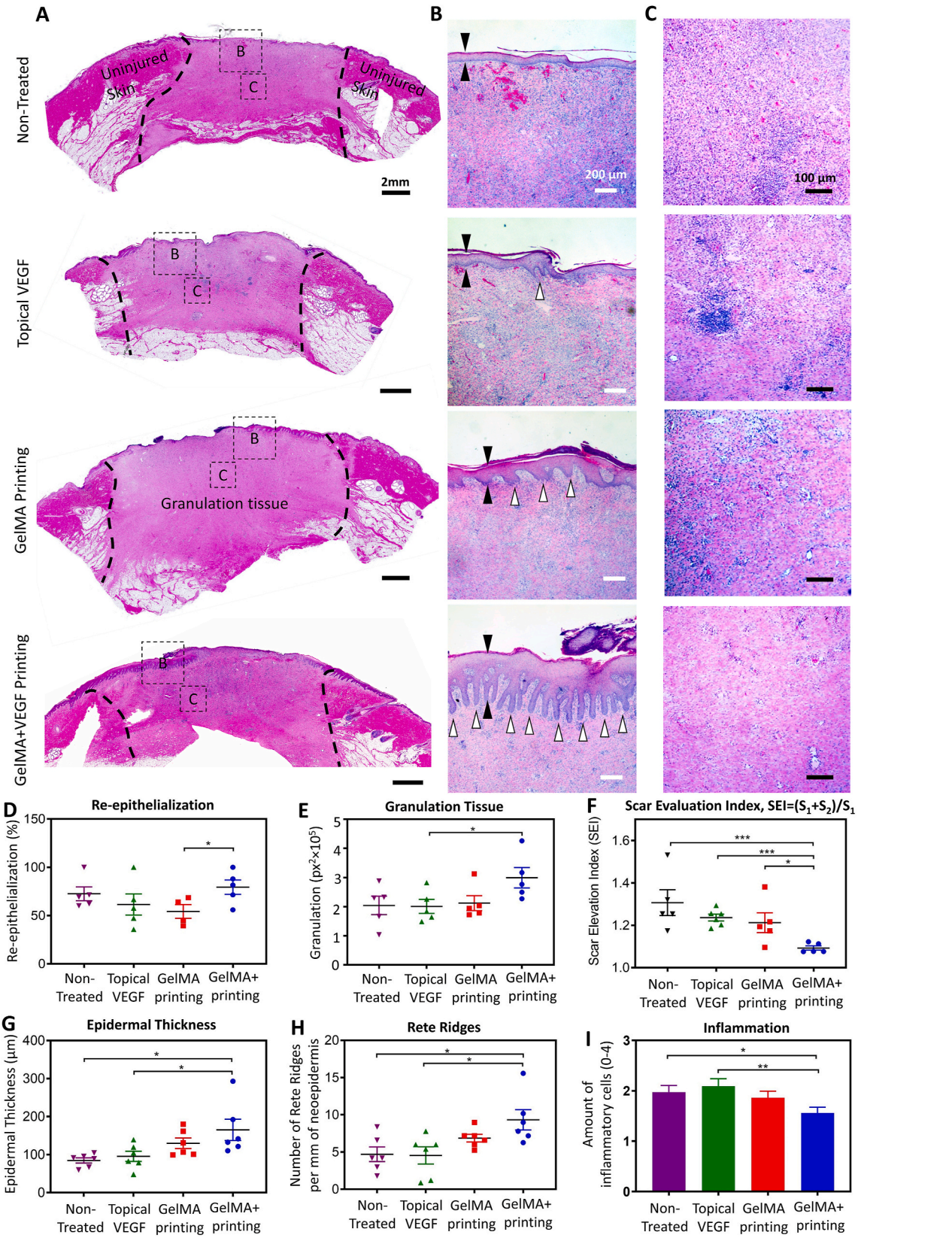

(caption on next page)

Fig. 5. Microscopic evaluation of wound healing quality. (A–C) Representative histology pictures of the wound area on day 14 post surgery. The whole wound area is shown in (A), while the epidermis and wound bed are shown in (B) and (C), respectively. Different groups are the wounds treated with (i) *in vivo* printed GelMA containing VEGF (GelMA + VEGF printing), (ii) *in vivo* printed blank GelMA (GelMA printing), (iii) BPS containing VEGF administrated topically (topical VEGF), and (iv) wounds left untreated (non-treated). A thicker epithelial layer, more rete ridges, and lower amount of infiltrative cells in the wound bed demonstrates a significantly higher quality of healing in the wounds treated GelMA + VEGF printing. (D–I) Quantitate analysis of wound healing quality. (D) Wound re-epithelialization, calculated based on the area of new epithelium over total wound area. Highest amount of re-epithelialization was observed in the wounds treated with GelMA + VEGF. (E) Amount of granulation tissue. The GelMA + VEGF treated wounds had the largest area of granulation tissue. (F) Scar elevation index (SEI), calculated based on the total area of the healed skin over the area of normal skin below the buildup hypertrophic scarring. The wounds treated with GelMA + VEGF demonstrated significantly less scarring compared to the other groups. (G) Epidermal thickness. The thickness of epidermis was increased in the wounds treated with the GelMA + VEGF. (H) Rete ridges. The number of rete ridges in the GelMA + VEGF group was significantly higher compared to the non-treated and VEGF treated wounds. (I) Inflammation. The degree of inflammation was studied by analyzing the H&E stained wound sections for infiltration of inflammatory cells to the wound bed (Representative figures are shown in (C)). The inflammation was present in all wounds while wounds treated with GelMA + VEGF contained the smallest number of inflammatory cells. n = 6 was considered for quantifications.

VEGF treated wounds. Wound contraction, a process where differentiated fibroblasts called myofibroblasts close the injured area by pulling the wound edges together, is an important part of normal wound healing. However, if the contraction is excessive and prolonged, it leads to scarring which can have a significant impact on the quality of life especially if the function and appearance of healed tissue are affected [73]. Currently, there is no established therapy to prevent excessive contraction and scarring, although novel tissue engineering approaches have shown some promise [63]. Contrary to our results, others have shown that VEGF may promote scar formation in the skin, although the mechanisms by which this happens is unclear [74]. The contradictory results may be due to differences in approach for drug delivery, as suggested previously [21]. Controlled spatiotemporal drug distribution can significantly affect the outcomes of growth factor therapies. In the present study, scaffold-mediated sustained VEGF delivery promotes wound healing.

Although less effective than GelMA containing VEGF bioink, the *in vivo* printing of blank GelMA also significantly reduced the contraction compared to the non-treated wounds. Previously, it has been shown that a moist wound environment significantly reduces scar formation and that hydrogel treatment might also prevent wound contraction [65,69]. In porcine full-thickness wounds, it was shown that application of a nanocellulose hydrogel prevented wound contraction as well as secondary contraction of a meshed split-thickness skin graft (STSG). Yet, no mechanism how this happens has been presented [65]. Here, in addition to sustaining the release rate, adhered GelMA can modulate the wound moisture, provide a scaffold for cell migration and ingrowth, and temporarily protect the wound bed before complete healing of the wound.

Immunohistochemical analysis further confirmed the benefit of *in vivo* printing of VEGF-eluting GelMA scaffolds on the angiogenesis and therefore the quality of wound healing (Fig. 6). To evaluate the amount of angiogenesis, the level of von Willebrand Factor (vWF), a protein highly expressed in endothelium, was measured in the wound bed (Fig. 6A). Qualitative (Fig. 6B and **C**) and quantitative outcomes demonstrated a significant increase in wound bed vascularization, within the depth of granulation tissue, as a result of *in vivo* printing of GelMA supplemented with VEGF. A sustained release of VEGF from the GelMA scaffold ensures the local availability of the VEGF throughout the wound healing process, which induces angiogenesis and therefore offers more advanced healing with minimum subsequent scarring. Noteworthy, the topical delivery of VEGF was clearly less effective, highlighting the importance of sustained delivery in the effectiveness of drugs and growth factors in wound healing (Fig. 6C). Additionally, immunostaning against cluster of differentiation 3 (CD3), a protein highly expressed on the T-cells, demonstrated insignificant immune response to the proposed treatment (Fig. S6). VEGF delivery was not expected to offer anti-inflammatory effect, specially in the acute and non-chronically inflamed wound model used here. However, the implemented scaffolding material did not lead to increase in the level of CD3 positive cells. While a statistically significant difference was not observed between the groups, there was a trend toward reduced immune

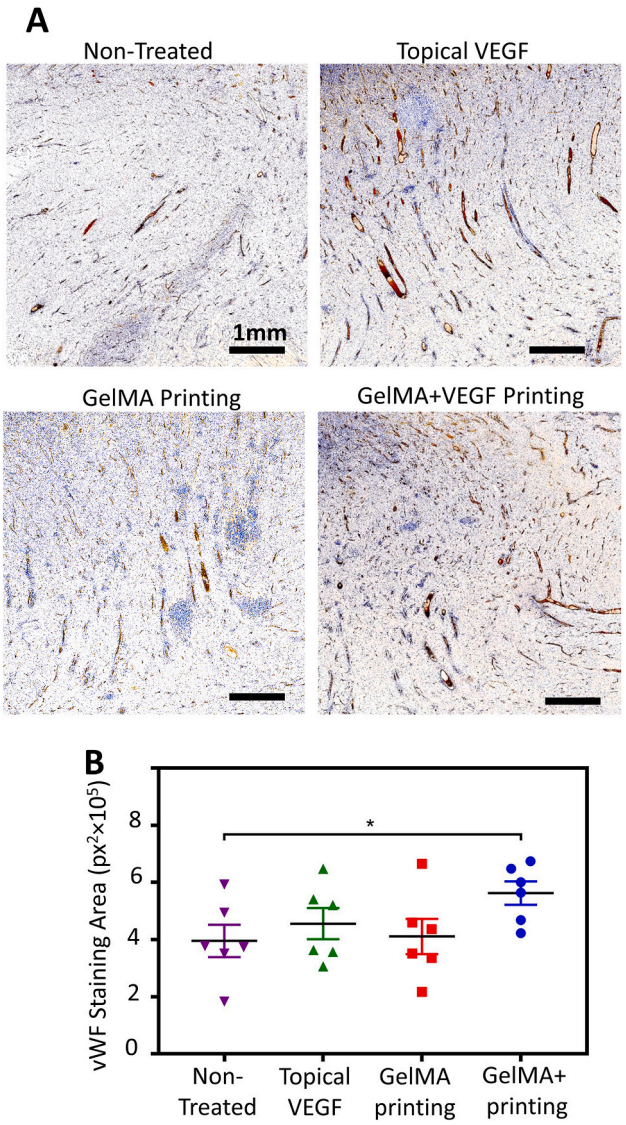

Fig. 6. Immunohistochemical analysis of angiogenesis in the wound bed on day 14 post surgery. The wound bed was examined for the expression of von Willebrand Factor (vWF). (A) Representative images of wound bed angiogenesis in non-treated wounds compared to those treated with BPS containing VEGF administrated topically (topical VEGF), *in vivo* printed blank GelMA (GelMA printing), and *in vivo* printed GelMA containing VEGF (GelMA + VEGF printing). The brown color indicates the presence of vWF. (B) Quantitative results of wound bed angiogenesis through measurement of vWF signal in different wounds (n = 6).

response in the wounds treated with *in vivo* printing of VEGF-eluting GelMA hydrogel, confirming the histological evaluations.

3. Conclusions

In conclusion, the hand-held 3D bioprinter has a great potential to deliver novel but also available and clinically valuable treatments for wound healing. The present study demonstrated successful *in vitro* and *in vivo* bioprinting of VEGF-loaded GelMA hydrogel. In the first phase of the study, the hydrogel characteristics were optimized *in vitro* to offer good printability, suitable tissue adhesion, and favorable environment for cellular function. Subsequently, the VEGF containing GelMA hydrogel was applied into full-thickness porcine wounds using the hand-held 3D bioprinter and its effects on wound closure and quality of healing were studied. It was observed that bioprinting of the GelMA hydrogel into the wounds was convenient and enabled rapid wound coverage. The application of the developed handheld printer enables printing into complex, irregularly shaped defects, while *in situ* cross-linking mechanism ensures the bioink is contained within the defect with homogeneous distribution over the wound area, particularly when printing onto curved defects. Furthermore, the strategy allows printing of the hydrogel to conform to the crevices and small corners of the wound, which enhances the hydrogel-tissue adhesion and subsequent integration. The results demonstrated that although no differences in wound closure were seen, the VEGF containing GelMA hydrogel increased the quality of healing in terms of less wound contraction, reduced scar formation and enhanced neoepidermis formation in comparison to control treatments. Interestingly, *in vivo* printing of blank GelMA as well as topical VEGF administration demonstrated limited effects on the wound healing quality, whereas the sustained release of VEGF from an *in vivo* printed scaffold with a simple but robust handheld printer could significantly enhance the wound bed angiogenesis and resulted in more advanced healing. While *in vivo* printed scaffolds clearly showed significant advantages in wound healing quality at day 14, additional studies that would investigate the impact of this treatment during all the different phases of wound healing are needed to comprehensively demonstrate the efficacy. Shorter studies are needed to assess the effect on inflammation, and longer term experiments are needed to assess the scarring after complete wound closure.

4. Experimental Section

4.1. Materials

GelMA with medium degree of methacrylation was purchased from Allevi (Cat: GMA) while Lithium phenyl-2,4,6-trimethylbenzoyl phosphinate (LAP) was obtained from Sigma (Cat: 900889) to be used as the photo-initiator. Recombinant human vascular endothelial growth factor A (VEGF-A, Bio-Rad, Cat: PHP293) was used for the *in vitro* scratch assay on human umbilical vein endothelial cells (HUVECs, Sigma, Cat: 200P–05 N). For culturing HUVECs, endothelial cell growth medium was obtained from Lonza (Cat: CC-3124) while Dulbecco's phosphate-buffered saline (DPBS, Gibco) was purchased from ThermoFisher Scientific. Matrigel was obtained from Fisher Scientific (Corning, Cat: CB40234) and used in the scratch assay. Rhodamine B (Rho-B, Sigma, Cat: R6626) and bovine serum albumin fluorescein isothiocyanate conjugate (BSA-FITC, Sigma, Cat: A9771) were implemented for assessment of release profile. Polydimethylsiloxane (PDMS) was purchased from Fisher Scientific (Sylgard 184, Cat: NC9285739).

4.2. Development and characterization of handheld bioprinter

The developed handheld printer was a miniaturized controllable syringe pump with embedded curing light [75]. A custom designed housing was designed in SolidWorks (Dassault Systèmes) and constructed using stereolithography in a Connex3 Object500 (Stratasys). Electronics were embedded within the housing and included a continuously variable speed controller (P160KN–0FC18C2K5, Digi-Key), directional toggle (3220, Adafruit), and photocrosslinking system. An electronic motor (Pololu) enabled extrusion of syringes filled with precursor hydrogels. The rotational motion of the motor was transferred to linear motion using a leadscrew. The linear motion was controlled by guiding shafts, enabling the reliable extrusion of the syringe plunger loaded into the device. A chargeable battery (2500 mAh, GTF) and power conservation mode were utilized to enable several hours of continuous operation. The crosslinking system was positioned 45 mm away from the extrusion nozzle tip and used a 1 W Blue light LED (395 nm wavelength, CH_Town Electronic) for photopolymerization.

The characterization of the printing parameters was perform through measurement of generated flowrates and calculation of the corresponding printing speed and filament diameter. A 9% GelMA was extruded through a gauge 22 conical nozzle to measure the flowrates in different motor power levels. The printing speed and corresponding filament diameter was then calculated and graphed for different flowrates.

4.3. Bioink preparation

To prepare the bioink, lyophilized GelMA was dissolved in pre-warmed DPBS with desired concentration, followed by addition of a 50X LAP solution (3.35% w/v in DPBS) with a 50:1 volumetric ratio. The VEGF was then supplemented and the solution was mixed by pipetting up and down to ensure a uniform distribution of LAP and VEGF throughout the hydrogel precursor. The preparation of the bioink was performed under a biosafety hood, using sterile reagents and materials. To ensure sterility, the bioink was preheated and filtered using syringe filters (0.22 μm pore size) into a 50 mL centrifuge tube and kept in warm bath (37 °C) before the experiments.

4.4. Mechanical characterization of GelMA ink

Compression tests were performed to evaluate the elastic modulus of the GelMA having different concentrations, as previously described [33]. A molded cylindrical hydrogel structure with a 10-mm diameter and 4.5 mm height was used as the sample for compression tests. A male master mold was first fabricated with corresponding dimensions using SLA 3D printing (ANYCUBIC, Photon S), followed by casting a PDMS female mold on top of it. Subsequently, a GelMA solution supplemented with 0.067% (w/v) LAP was filled inside the PDMS mold, capped with a charged glass slide (Fisher Scientific, Cat: 99-910-01) and photo-crosslinked through the slide using a UV light (Jowbeam) for 20 s from a distance of 4 cm. The hydrogel cylinder was then removed from the mold and placed between compression plates mounted on a mechanical testing device (Model: 3220-TA Series III, TA Instruments), as shown in Fig. 3A. A compression rate of 0.1 mm/s was then applied and the elastic modulus was calculated from the slope of a fitted line interpolating the stress-strain data up to 10% strain.

4.5. Assessment of adhesion of in situ printed scaffolds

For evaluating adhesion strength of GelMA to pig skin, a shear test was performed based on ASTM F2255-05 standard [76]. A rectangular piece of pig skin (10 mm × 20 mm) was cut and glued to a coverslip using cyanoacrylate adhesive. Then GelMA was printed on the pig skin, a charged glass slide was placed on top of it, and GelMA was crosslinked for 20 s. As shown in Fig. 2B, the sample was then secured on the mechanical testing device using grips and pulled in shear at a rate of 0.1 mm/s until failure occurred.

4.6. Scanning electron microscopy

For scanning electron microscopy (SEM) analysis, 9% (w/v) GelMA

hydrogel was printed on a cut piece of pig skin and photo-crosslinked for 20 s. The sample was then dropped into a liquid nitrogen bath to snap freeze the hydrogel and was immediately placed inside a freeze dryer (FreeZone 2.5 L −50C Benchtop, Labconco) to lyophilize for 24 h. The sample was then broken to expose the cross-section for imaging the internal structure of the hydrogel. The cross-section was mounted on a stub and coated with gold using a sputter coater device (Vacuum Desk V, Denton) for 60 s at 20 mA. A benchtop SEM (TM-1000, HITACHI) was then used to capture the images.

4.7. Evaluation of VEGF release profile

GelMA precursor (9% w/v) was supplemented with VEGF (400 ng/ml) and added to 8 μm pore 24-well Falcon® cell culture inserts (Corning), followed by its crosslinking for 20 s (n = 4). Blank GelMA was used as the control group in the experiments (n = 4). The inserts were then placed into 24-well plates containing 600 μL of DPBS per well. The plates were placed in an incubating shaker (Fisherbrand™, Fisher Scientific) at 37 °C. At each time-point, the DPBS solutions were collected from the wells and replaced with fresh DPBS. After collection, the solutions were stored at −20 °C. The concentrations of VEGF in the solutions were measured using an enzyme-linked immunosorbent assay (ELISA) kit (900-K10, Peprotech) as per manufacturer-recommended protocol and the signals were measured using a plate reader (Cytation 5, Biotek).

4.8. Western blot

Western blot test was performed using sodium dodecyl sulphate-polyacrylamide gel electrophoresis (SDS-PAGE). Samples (30 μL of the collected samples from day 7 of the release study with 30 μL of 2X sample buffer per well) were electrophoresed on 4–20% Tris-Glycine gels (Invitrogen, Carlsbad, CA), followed by electroblotting to a PVDF membrane. The membrane was then blocked in 5% non-fat dry milk (Biorad, Hercules, CA) in Tris-buffered saline + 0.05% Tween-20 (TBST) for 1h at room temperature. Membranes were then probed with anti-VEGF antibody (1:600, 19003-1-AP, Thermo Fischer Scientific, Waltham, MA) in 3% non-fat dry milk in TBST overnight at 4 °C. After washing with TBST, membranes were incubated with goat-anti-rabbit HRP-conjugated secondary antibody (1:10000, MilliporeSigma, Burlington, MA) for 1 h in 3% non-fat dry milk in TBST at room temperature, washed in TBST again, then imaged on a G:Box Chemi XX9 imager (Syngene, Frederick, MD) using SuperSignal West Femto (Thermo Fisher Scientific, Waltham, MA).

4.9. In vitro scratch assay

A scratch assay was performed to evaluate the effect of VEGF released from the GelMA scaffold on the functionality of the endothelial cells (Fig. 3A). HUVECs were subcultured up to passage 4 by detaching the cells using Trypsin-EDTA (Gibco) and resuspending in growth medium. A 12-well plate was coated with 5% (v/v) Matrigel overnight, washed with DPBS, and then seeded with HUVECs at a concentration of 1×10^5 cell/well. Upon HUVECs confluency, a 200 μL pipette tip was used to gently scratch the confluent HUVECs layer and make a ~350 μm gap in the cell monolayer.

Following the induction of the scratch, different treatment conditions were used: (i) cell culture inserts without a filling reagent (negative control), (ii) cell culture inserts filled with 200 μL of pure GelMA, (iii) cell culture inserts filled with 200 μL of GelMA supplemented with 400 ng/ml VEGF, and (iv) cell culture inserts filled with 200 μL of media supplemented with 400 ng/mL VEGF (positive control). GelMA was photo-crosslinked for 20 s, and the cell culture inserts were place inside the cell-seeded wells containing growth media and imaged every 2 h to monitor the gap closure. The gap area was then measured using FIJI open-source software and normalized to the initial gap area [77].

4.10. Animal study

The procedures were performed at Toxikon Corporation (Bedford, MA). The study protocol was approved by Toxikon's Institutional Animal Care and Use Committee, and conformed to federal animal laws and regulations (Project ID number 19-04108-N2). Three Yorkshire pigs (Animal Biotech Industries, Danboro, PA) weighing between 70 and 80 kg were used in the study. Anesthesia was induced with intramuscular administration of 3.3 mg/kg ketamine, 1.1 mg/kg acepromazine, 2.2 mg/kg xylazine and 0.02 mg/kg atropine. General anesthesia was maintained with 0–5% isoflurane and oxygen. After the procedure, a transdermal patch releasing 2–3 mkg/kg/h fentanyl per hour for 72 h (Duralgesic, Janssen) was given for pain management during surgical recovery and buprenorphine 0.01–0.03 mg/kg was administered IM immediately at the end of the procedure.

Circular full-thickness wounds (d = 1 inch) were created on the dorsum of each pig using sterile scalpel [60]. After marking the wounds in parallel paraspinal stripes, the outlines were tattooed with red ink using an electric tattoo marker (Spaulding & Rogers Manaufacturing Inc., Voorheesville, NY). Full-thickness wounds down to fascia were excised. Wounds were separated by at least 4 cm of unwounded skin. After wound creation, the wounds were randomly divided into 4 treatment groups (n = 6): 1) *In situ* printed GelMA scaffolds containing VEGF; 2) *in situ* printed GelMA scaffolds without VEGF; 3) topical delivery of VEGF in PBS, and 4) non-treated (negative control). For all treatment groups, 1 ml of the therapeutic was administrated. The therapeutic was GelMA 9%, GelMA 9% supplemented with 400 ng/ml VEGF, and PBS supplemented with 400 ng/ml VEGF, respectively for groups 1 to 3. We have previously verified this VEGF dosage required for induction of endothelial cell migration and consequent vascularization *in vitro* and *in vivo* [4,60]. We have been previously demonstrated that administration of 100 μL VEGF (500 ng/mL) solution at two time points throughout the healing process can accelerate the wound (1 cm2) healing in mice, while 400 μL VEGF at the same concentration and administration frequency can improve porcine wound (5 cm2) healing. A similar dosage was used in this study for porcine wound healing. For *in vivo* printing groups (groups 1 and 2), the printing followed a spiral pattern to fill the entire wound bed. Subsequently all the wounds were covered independently with a semipermeable film dressing (Tegaderm, 3 M, Saint Paul, MN). On day 7 post operatively, the dressings were changed. On postoperative day 14, the animals were euthanized and the wounds were photographed and harvested for histology. A 14-day long experiment was designed for this study because it has been shown that acute wounds in healthy young pigs heal very efficiently. Fig. S4 illustrates the workflow of the animal study.

4.10.1. Macroscopic wound closure

The wounds were photographed on day 0 after wound creation, on day 7 during dressing changes and on day 14 after euthanasia. Macroscopic wound closure was also calculated from the photos using Image J software (NIH, Bethesda, MD). The area of the remaining open wound was measured and compared to the wound area at day 0 and expressed as a percentage of its original size. Wound contraction was measured of the tattooed margins from macroscopic wound photos using Image J software (NIH). The area inside the tattooed line was measured and expressed as a percentage of its original size on day 0 [78–80].

4.10.2. Microscopic evaluation

The excised wounds were fixed in formalin, embedded in paraffin, cut in sections to give a cross section view of the wound edge-to-edge and stained with hematoxylin and eosion (H&E). The slides were analyzed for inflammatory infiltrate using the following score scale: 4 = marked, 3 = moderate, 2 = minimal, and 1 = absent. The amount of granulation tissue was measured from the total wound area at day 14. Re-epithelialization was quantified as the area of the new epithelium divided by the wound area. The degree of scar hypertrophy was

calculated using scar elevation index (SEI) that represents the ratio of the total wound area tissue height to the area of normal tissue below the hypertrophic scar. A SEI of 1 represents no scarring while higher number represents increased scarring. Epidermal thickness was measured in 5 representative areas of neoepidermis for each wound cross-section. The number of rete ridges per millimeter of neoepithelium was counted under the microscope from 5 standardized locations in each wound after 14 days of healing. All the analyses were performed in a blinded fashion.

4.10.3. Immunohistochemistry staining

The fixed and paraffin embedded tissues were cut in sections to give a cross section view of the wound edge-to-edge. The wound sections were immunostained for von Willebrand Factor (vWF; 0082, Dako), based on manufacturers' protocols and imaged using a light microscope. The amount of positive staining was quantified in a blinded-manner in Image J software.

4.11. Statistical analyses

Data analyses were done using GraphPad Prism 6.0 software (Graph Pad software Inc. La Jolla, CA). Comparison of the different groups was performed using a student's T test and values $P < 0.05$ were considered statistically significant. The *in vitro* data are presented as mean ± standard deviation. The data related to animal studies is presented as mean ± standard error of mean (SEM). *, **, *** and **** represent $P < 0.05$, $P < 0.005$, $P < 0.0005$ and $P < 0.00005$, respectively. N-number for each group was 6 while 3 biological replicates (number of animals) was considered in animal studies.

Supporting information

The printability of GelMA with different concentration (Fig. S1), the SEM analysis of samples prepared using critical point drying (Fig. S2), the western blot analysis of released VEGF from the hydrogel (Fig. S3), the workflow of the animal studies (Fig. S4), the schematic representation of SEI calculation method (Fig. S5), and immunohistological analysis of the wound bed to assess the level of immune response to the applied treatments (Fig. S6) are available in supporting information.

Author contributions

K. Nuutila and M. Samandari contributed equally to the work.

CRediT authorship contribution statement

Kristo Nuutila: Formal analysis, contributed equally to this work, conceived the idea, performed the animal studies, data analysis and interpretation of the results. **Mohamadmahdi Samandari:** contributed equally to this work, designed the handheld printer and characterized the printability of GelMA ink, characterized the physical properties of the scaffolds and the release kinetics of VEGF and its function in vitro, performed the animal studies. **Yori Endo:** performed the animal studies. **Yuteng Zhang:** performed the animal studies. **Jacob Quint:** designed the handheld printer and characterized the printability of GelMA ink, characterized the physical properties of the scaffolds and the release kinetics of VEGF and its function in vitro. **Tannin A. Schmidt:** characterized the physical properties of the scaffolds and the release kinetics of VEGF and its function in vitro. **Ali Tamayol:** conceived the idea, performed the animal studies, assisted with the data analysis and interpretation of the results. **Indranil Sinha:** conceived the idea, assisted with the data analysis and interpretation of the results. The manuscript was written and revised by all authors.

Declaration of competing interest

The authors declare that they have no known competing financial interests or personal relationships that could have appeared to influence the work reported in this paper.

Acknowledgment

Paige Woods is gratefully acknowledged for her technical assistance with western blot. The financial support from the National Institutes of Health (GM126831, AR073822) and Stepping Strong Innovator Award are gratefully acknowledged. Kristo Nuutila, Mohamadmahdi Samandari, Jacob Quint, Ali Tamayol, and Indranil Sinha declare financial interest in Inprint Bio Ltd.

Appendix A. Supplementary data

Supplementary data to this article can be found online at https://doi.org/10.1016/j.bioactmat.2021.06.030.

References

[1] J.E. Calonje, T. Brenn, A.J. Lazar, S.D. Billings, McKee's pathology of the skin, vol. 2 Volume Set E-Book, Elsevier Health Sciences2018.
[2] L. Barnum, M. Samandari, T.A. Schmidt, A. Tamayol, Microneedle arrays for the treatment of chronic wounds, Expet Opin. Drug Deliv. 17 (12) (2020) 1767–1780.
[3] G.C. Gurtner, S. Werner, Y. Barrandon, M.T. Longaker, Wound repair and regeneration, Nature 453 (7193) (2008) 314–321.
[4] H. Derakhshandeh, F. Aghabaglou, A. McCarthy, A. Mostafavi, C. Wiseman, Z. Bonick, I. Ghanavati, S. Harris, C. Kreikemeier-Bower, S.M. Moosavi Basri, J. Rosenbohm, R. Yang, P. Mostafalu, D. Orgill, A. Tamayol, A wirelessly controlled smart bandage with 3D-printed miniaturized needle arrays, Adv. Funct. Mater. 30 (13) (2020) 1905544.
[5] J.J. Tomasek, G. Gabbiani, B. Hinz, C. Chaponnier, R.A. Brown, Myofibroblasts and mechano-regulation of connective tissue remodelling, Nat. Rev. Mol. Cell Biol. 3 (5) (2002) 349–363.
[6] S.A. Eming, P. Martin, M. Tomic-Canic, Wound repair and regeneration: mechanisms, signaling, and translation, Sci. Transl. Med. 6 (265) (2014), 265sr6-265sr6.
[7] S.R. Nussbaum, M.J. Carter, C.E. Fife, J. DaVanzo, R. Haught, M. Nusgart, D. Cartwright, An economic evaluation of the impact, cost, and medicare policy implications of chronic nonhealing wounds, Value Health 21 (1) (2018) 27–32.
[8] C.K. Sen, Human Wounds and its Burden: an Updated Compendium of Estimates, Mary Ann Liebert, Inc., publishers 140 Huguenot Street, 3rd Floor New, 2019.
[9] I. Jones, L. Currie, R. Martin, A guide to biological skin substitutes, Br. J. Plast. Surg. 55 (3) (2002) 185–193.
[10] S. Saghazadeh, C. Rinoldi, M. Schot, S.S. Kashaf, F. Sharifi, E. Jalilian, K. Nuutila, G. Giatsidis, P. Mostafalu, H. Derakhshandeh, K. Yue, W. Swieszkowski, A. Memic, A. Tamayol, A. Khademhosseini, Drug delivery systems and materials for wound healing applications, Adv. Drug Deliv. Rev. 127 (2018) 138–166.
[11] A. Tamayol, M. Akbari, Y. Zilberman, M. Comotto, E. Lesha, L. Serex, S. Bagherifard, Y. Chen, G.Q. Fu, S.K. Ameri, W.T. Ruan, E.L. Miller, M.R. Dokmeci, S. Sonkusale, A. Khademhosseini, Flexible pH-sensing hydrogel fibers for epidermal applications, Adv Healthc Mater 5 (6) (2016) 711–719.
[12] P. Mostafalu, A. Tamayol, R. Rahimi, M. Ochoa, A. Khalilpour, G. Kiaee, I.K. Yazdi, S. Bagherifard, M.R. Dokmeci, B. Ziaie, S.R. Sonkusale, A. Khademhosseini, Smart Bandage for Monitoring and Treatment of Chronic Wounds, 2018, e1703509. Small.
[13] M. Comotto, S. Saghazadeh, S. Bagherifard, B. Aliakbarian, M. Kazemzadeh-Narbat, F. Sharifi, S.A. Mousavi Shaegh, E. Arab-Tehrany, N. Annabi, P. Perego, Breathable hydrogel dressings containing natural antioxidants for management of skin disorders, J. Biomater. Appl. 33 (9) (2019) 1265–1276.
[14] J. Koehler, F.P. Brandl, A.M. Goepferich, Hydrogel wound dressings for bioactive treatment of acute and chronic wounds, Eur. Polym. J. 100 (2018) 1–11.
[15] K. Elkhoury, C.S. Russell, L. Sanchez-Gonzalez, A. Mostafavi, T.J. Williams, C. Kahn, N.A. Peppas, E. Arab-Tehrany, A. Tamayol, Soft-nanoparticle functionalization of natural hydrogels for tissue engineering applications, Advanced Healthcare Materials 8 (18) (2019) 1900506.
[16] B.V. Slaughter, S.S. Khurshid, O.Z. Fisher, A. Khademhosseini, N.A. Peppas, Hydrogels in regenerative medicine, Adv. Mater. 21 (32-33) (2009) 3307–3329.
[17] M. Samandari, F. Alipanah, S. Haghjooy Javanmard, A. Sanati-Nezhad, One-step wettability patterning of PDMS microchannels for generation of monodisperse alginate microbeads by in Situ external gelation in double emulsion microdroplets, Sensor. Actuator. B Chem. 291 (2019) 418–425.
[18] H. Derakhshandeh, S.S. Kashaf, F. Aghabaglou, I.O. Ghanavati, A. Tamayol, Smart bandages: the future of wound care, Trends Biotechnol. 36 (12) (2018) 1259–1274.
[19] K. Nuutila, J. Grolman, L. Yang, M. Broomhead, S. Lipsitz, A. Onderdonk, D. Mooney, E. Eriksson, Immediate treatment of burn wounds with high concentrations of topical antibiotics in an alginate hydrogel using a platform wound device, Adv. Wound Care 9 (2) (2020) 48–60.
[20] L. Yang, M. Broomhead, K. Nuutila, K. Proppe, E. Eriksson, Topically delivered minocycline penetrates a full-thickness burn eschar and reduces tissue bacterial counts, J. Burn Care Res. 39 (5) (2018) 790–797.

[21] K. Lee, E.A. Silva, D.J. Mooney, Growth factor delivery-based tissue engineering: general approaches and a review of recent developments, J. R. Soc. Interface 8 (55) (2011) 153–170.

[22] Y. Sun, D. Nan, H. Jin, X. Qu, Recent advances of injectable hydrogels for drug delivery and tissue engineering applications, Polym. Test. 81 (2020) 106283.

[23] A. Smandri, A. Nordin, N.M. Hwei, K.-Y. Chin, I. Abd Aziz, M.B. Fauzi, Natural 3D-printed bioinks for skin regeneration and wound healing: a systematic review, Polymers 12 (8) (2020) 1782.

[24] S.P. Tarassoli, Z.M. Jessop, A. Al-Sabah, N. Gao, S. Whitaker, S. Doak, I. S. Whitaker, Skin tissue engineering using 3D bioprinting: an evolving research field, J. Plast. Reconstr. Aesthetic Surg. 71 (5) (2018) 615–623.

[25] S. Singh, D. Choudhury, F. Yu, V. Mironov, M.W. Naing, In situ bioprinting–Bioprinting from benchside to bedside? Acta Biomater. 101 (2020) 14–25.

[26] S. Ostrovidov, S. Salehi, M. Costantini, K. Suthiwanich, M. Ebrahimi, R. B. Sadeghian, T. Fujie, X. Shi, S. Cannata, C. Gargioli, 3D bioprinting in skeletal muscle tissue engineering, Small 15 (24) (2019) 1805530.

[27] I.T. Ozbolat, Bioprinting scale-up tissue and organ constructs for transplantation, Trends Biotechnol. 33 (7) (2015) 395–400.

[28] X. Li, Q. Lian, D. Li, H. Xin, S. Jia, Development of a robotic arm based hydrogel additive manufacturing system for in-situ printing, Appl. Sci. 7 (1) (2017).

[29] S. Singh, D. Choudhury, F. Yu, V. Mironov, M.W. Naing, In situ bioprinting – bioprinting from benchside to bedside? Acta Biomater. 101 (2020) 14–25.

[30] A. Skardal, D. Mack, E. Kapetanovic, A. Atala, J.D. Jackson, J. Yoo, S. Soker, Bioprinted amniotic fluid-derived stem cells accelerate healing of large skin wounds, STEM CELLS Translational Medicine 1 (11) (2012) 792–802.

[31] M. Albanna, K.W. Binder, S.V. Murphy, J. Kim, S.A. Qasem, W. Zhao, J. Tan, I.B. El-Amin, D.D. Dice, J. Marco, J. Green, T. Xu, A. Skardal, J.H. Holmes, J.D. Jackson, A. Atala, J.J. Yoo, In situ bioprinting of autologous skin cells accelerates wound healing of extensive excisional full-thickness wounds, Sci. Rep. 9 (1) (2019) 1856.

[32] N. Hakimi, R. Cheng, L. Leng, M. Sotoudehfar, P.Q. Ba, N. Bakhtyar, S. Amini-Nik, M.G. Jeschke, A. Günther, Handheld skin printer: in situ formation of planar biomaterials and tissues, Lab Chip 18 (10) (2018) 1440–1451.

[33] C.S. Russell, A. Mostafavi, J.P. Quint, A.C. Panayi, K. Baldino, T.J. Williams, J. G. Daubendiek, V. Hugo Sánchez, Z. Bonick, M. Trujillo-Miranda, S.R. Shin, O. Pourquie, S. Salehi, I. Sinha, A. Tamayol, In situ printing of adhesive hydrogel scaffolds for the treatment of skeletal muscle injuries, ACS Applied Bio Materials 3 (3) (2020) 1568–1579.

[34] G. Ying, J. Manríquez, D. Wu, J. Zhang, N. Jiang, S. Maharjan, D.H. Hernández Medina, Y.S. Zhang, An open-source handheld extruder loaded with pore-forming bioink for in situ wound dressing, Materials Today Bio 8 (2020) 100074.

[35] S. Duchi, C. Onofrillo, C.D. O'Connell, R. Blanchard, C. Augustine, A.F. Quigley, R. M.I. Kapsa, P. Pivonka, G. Wallace, C. Di Bella, P.F.M. Choong, Handheld Co-Axial Bioprinting: application to in situ surgical cartilage repair, Sci. Rep. 7 (1) (2017) 5837.

[36] C. Di Bella, S. Duchi, C.D. O'Connell, R. Blanchard, C. Augustine, Z. Yue, F. Thompson, C. Richards, S. Beirne, C. Onofrillo, S.H. Bauquier, S.D. Ryan, P. Pivonka, G.G. Wallace, P.F. Choong, In situ handheld three-dimensional bioprinting for cartilage regeneration, Journal of Tissue Engineering and Regenerative Medicine 12 (3) (2018) 611–621.

[37] C.D. O'Connell, C. Di Bella, F. Thompson, C. Augustine, S. Beirne, R. Cornock, C. J. Richards, J. Chung, S. Gambhir, Z. Yue, J. Bourke, B. Zhang, A. Taylor, A. Quigley, R. Kapsa, P. Choong, G.G. Wallace, Development of the Biopen: a handheld device for surgical printing of adipose stem cells at a chondral wound site, Biofabrication 8 (1) (2016), 015019.

[38] R.Y. Cheng, G. Eylert, J.-M. Gariepy, S. He, H. Ahmad, Y. Gao, S. Priore, N. Hakimi, M.G. Jeschke, A. Günther, Handheld instrument for wound-conformal delivery of skin precursor sheets improves healing in full-thickness burns, Biofabrication 12 (2) (2020), 025002.

[39] J. Li, D.J. Mooney, Designing hydrogels for controlled drug delivery, Nature Reviews Materials 1 (12) (2016) 1–17.

[40] N. Faramarzi, I.K. Yazdi, M. Nabavinia, A. Gemma, A. Fanelli, A. Caizzone, L. M. Ptaszek, I. Sinha, A. Khademhosseini, J.N. Ruskin, A. Tamayol, Patient-specific bioinks for 3D bioprinting of tissue engineering scaffolds, Advanced Healthcare Materials 7 (11) (2018) 1701347.

[41] M.G. Tonnesen, X. Feng, R.A.F. Clark, Angiogenesis in wound healing, J. Invest. Dermatol. Symp. Proc. 5 (1) (2000) 40–46.

[42] Z. Xie, C.B. Paras, H. Weng, P. Punnakitikashem, L.-C. Su, K. Vu, L. Tang, J. Yang, K.T. Nguyen, Dual growth factor releasing multi-functional nanofibers for wound healing, Acta Biomater. 9 (12) (2013) 9351–9359.

[43] P. Losi, E. Briganti, C. Errico, A. Lisella, E. Sanguinetti, F. Chiellini, G. Soldani, Fibrin-based scaffold incorporating VEGF- and bFGF-loaded nanoparticles stimulates wound healing in diabetic mice, Acta Biomater. 9 (8) (2013) 7814–7821.

[44] M.M. Hasani-Sadrabadi, P. Sarrion, S. Pouraghaei, Y. Chau, S. Ansari, S. Li, T. Aghaloo, A. Moshaverinia, An engineered cell-laden adhesive hydrogel promotes craniofacial bone tissue regeneration in rats, Sci. Transl. Med. 12 (534) (2020), eaay6853.

[45] K. Yue, G. Trujillo-de Santiago, M.M. Alvarez, A. Tamayol, N. Annabi, A. Khademhosseini, Synthesis, properties, and biomedical applications of gelatin methacryloyl (GelMA) hydrogels, Biomaterials 73 (2015) 254–271.

[46] S.R. Shin, H. Bae, J.M. Cha, J.Y. Mun, Y.-C. Chen, H. Tekin, H. Shin, S. Farshchi, M. R. Dokmeci, S. Tang, A. Khademhosseini, Carbon nanotube reinforced hybrid microgels as scaffold materials for cell encapsulation, ACS Nano 6 (1) (2012) 362–372.

[47] M. Samandari, F. Alipanah, K. Majidzadeh-A, M.M. Alvarez, G. Trujillo-de Santiago, A. Tamayol, Controlling cellular organization in bioprinting through designed 3D microcompartmentalization, Appl. Phys. Rev. 8 (2) (2021), 021404.

[48] N. Ashammakhi, S. Ahadian, C. Xu, H. Montazerian, H. Ko, R. Nasiri, N. Barros, A. Khademhosseini, Bioinks and bioprinting technologies to make heterogeneous and biomimetic tissue constructs, Materials Today Bio 1 (2019) 100008.

[49] K. Hölzl, S. Lin, L. Tytgat, S. Van Vlierberghe, L. Gu, A. Ovsianikov, Bioink properties before, during and after 3D bioprinting, Biofabrication 8 (3) (2016), 032002.

[50] F.J. O'Brien, Biomaterials & scaffolds for tissue engineering, Mater. Today 14 (3) (2011) 88–95.

[51] N. Cubo, M. Garcia, J.F. Del Cañizo, D. Velasco, J.L. Jorcano, 3D bioprinting of functional human skin: production and in vivo analysis, Biofabrication 9 (1) (2016), 015006.

[52] J. Yin, M. Yan, Y. Wang, J. Fu, H. Suo, 3D bioprinting of low-concentration cell-laden gelatin methacrylate (GelMA) bioinks with a two-step cross-linking strategy, ACS Appl. Mater. Interfaces 10 (8) (2018) 6849–6857.

[53] W. Liu, M.A. Heinrich, Y. Zhou, A. Akpek, N. Hu, X. Liu, X. Guan, Z. Zhong, X. Jin, A. Khademhosseini, Y.S. Zhang, Extrusion bioprinting of shear-thinning gelatin methacryloyl bioinks, Advanced Healthcare Materials 6 (12) (2017) 1601451.

[54] J.W. Nichol, S.T. Koshy, H. Bae, C.M. Hwang, S. Yamanlar, A. Khademhosseini, Cell-laden microengineered gelatin methacrylate hydrogels, Biomaterials 31 (21) (2010) 5536–5544.

[55] S.M. Naseer, A. Manbachi, M. Samandari, P. Walch, Y. Gao, Y.S. Zhang, F. Davoudi, W. Wang, K. Abrinia, J.M. Cooper, Surface acoustic waves induced micropatterning of cells in gelatin methacryloyl (GelMA) hydrogels, Biofabrication 9 (1) (2017), 015020.

[56] E. Shirzaei Sani, A. Kheirkhah, D. Rana, Z. Sun, W. Foulsham, A. Sheikhi, A. Khademhosseini, R. Dana, N. Annabi, Sutureless repair of corneal injuries using naturally derived bioadhesive hydrogels, Science Advances 5 (3) (2019), eaav1281.

[57] A. Assmann, A. Vegh, M. Ghasemi-Rad, S. Bagherifard, G. Cheng, E.S. Sani, G. U. Ruiz-Esparza, I. Noshadi, A.D. Lassaletta, S. Gangadharan, A. Tamayol, A. Khademhosseini, N. Annabi, A highly adhesive and naturally derived sealant, Biomaterials 140 (2017) 115–127.

[58] N. Annabi, D. Rana, E. Shirzaei Sani, R. Portillo-Lara, J.L. Gifford, M.M. Fares, S. M. Mithieux, A.S. Weiss, Engineering a sprayable and elastic hydrogel adhesive with antimicrobial properties for wound healing, Biomaterials 139 (2017) 229–243.

[59] M. Samandari, L. Rafiee, F. Alipanah, A. Sanati-Nezhad, S.H. Javanmard, A simple, low cost and reusable microfluidic gradient strategy and its application in modeling cancer invasion, Sci. Rep. 11 (1) (2021) 10310.

[60] M. Samandari, F. Aghabaglou, K. Nuutila, H. Derakhshandeh, Y. Zhang, Y. Endo, S. Harris, L. Barnum, C. Kreikemeier-Bower, E. Arab-Tehrany, N.A. Peppas, I. Sinha, A. Tamayol, Miniaturized needle array-mediated drug delivery accelerates wound healing, Advanced Healthcare Materials 10 (2021) 2001800.

[61] G. Gabbiani, The myofibroblast in wound healing and fibrocontractive diseases, J. Pathol.: A Journal of the Pathological Society of Great Britain and Ireland 200 (4) (2003) 500–503.

[62] H.D. Zomer, A.G. Trentin, Skin wound healing in humans and mice: challenges in translational research, J. Dermatol. Sci. 90 (1) (2018) 3–12.

[63] J.R. Sharpe, Y. Martin, Strategies demonstrating efficacy in reducing wound contraction in vivo, Adv. Wound Care 2 (4) (2013) 167–175.

[64] D.T. Corr, D.A. Hart, Biomechanics of scar tissue and uninjured skin, Adv. Wound Care 2 (2) (2013) 37–43.

[65] K. Nuutila, A. Laukkanen, A. Lindford, S. Juteau, M. Nuopponen, J. Vuola, E. Kankuri, Inhibition of skin wound contraction by nanofibrillar cellulose hydrogel, Plast. Reconstr. Surg. 141 (3) (2018) 357e–366e.

[66] M.J. Reid, L.J. Currie, S. Elizabeth James, J.R. Sharpe, Effect of artificial dermal substitute, cultured keratinocytes and split thickness skin graft on wound contraction, Wound Repair Regen. 15 (6) (2007) 889–896.

[67] R.R. Reid, N. Roy, J.E. Mogford, H. Zimmerman, C. Lee, T.A. Mustoe, Reduction of hypertrophic scar via retroviral delivery of a dominant negative TGF-β receptor II, J. Plast. Reconstr. Aesthetic Surg. 60 (1) (2007) 64–72.

[68] K. Nuutila, E. Eriksson, Moist wound healing with commonly available dressings, Adv. Wound Care (2020).

[69] R.G. Reish, B. Zuhaili, J. Bergmann, P. Aflaki, T. Koyama, F. Hackl, E. Waisbren, J. A. Canseco, K.D. Verma, E. Eriksson, Modulation of scarring in a liquid environment in the Yorkshire pig, Wound Repair Regen. 17 (6) (2009) 806–816.

[70] K. Breuing, E. Eriksson, P. Liu, D.R. Miller, Healing of partial thickness porcine skin wounds in a liquid environment, J. Surg. Res. 52 (1) (1992) 50–58.

[71] P.M. Vogt, C. Andree, K. Breuing, P.Y. Liu, J. Slama, G. Helo, E. Eriksson, Dry, moist, and wet skin wound repair, Ann. Plast. Surg. 34 (5) (1995) 493–500.

[72] K.E. Johnson, T.A. Wilgus, Vascular endothelial growth factor and angiogenesis in the regulation of cutaneous wound repair, Adv. Wound Care 3 (10) (2014) 647–661.

[73] B. Nedelec, A. Ghahary, P.G. Scott, E.E. Tredget, Control of wound contraction. Basic and clinical features, Hand Clin. 16 (2) (2000) 289–302.

[74] T.A. Wilgus, Vascular endothelial growth factor and cutaneous scarring, Adv. Wound Care 8 (12) (2019) 671–678.

[75] J. Quint, A. Mostafavi, Y. Endo, A. Panayi, C.S. Russell, A. Nourmahnad, C. Wiseman, L. Abbasi, M. Samandari, A. Sheikhi, K. Nuutila, I. Sinha, A. Tamayol, In vivo printing of nanoenabled scaffolds for the treatment of skeletal muscle injuries, Advanced healthcare materials 10 (2021) 2002152.

[76] ASTM F22255-03, Test Method for Strength Properties of Tissue Adhesives in Lap-Shear by Tension Loading, ASTM Internatational, West Conshohocken, PA, 2003.

[77] J. Schindelin, I. Arganda-Carreras, E. Frise, V. Kaynig, M. Longair, T. Pietzsch, S. Preibisch, C. Rueden, S. Saalfeld, B. Schmid, J.-Y. Tinevez, D.J. White, V. Hartenstein, K. Eliceiri, P. Tomancak, A. Cardona, Fiji: an open-source platform for biological-image analysis, Nat. Methods 9 (7) (2012) 676–682.

[78] R.K. Chan, L.F. Rose, J.C. Wu, D.I. Tucker, M.M. Chan, R.J. Christy, R.G. Hale, K. P. Leung, Autologous graft thickness affects scar contraction and quality in a porcine excisional wound model, Plastic and Reconstructive Surgery Global Open 3 (7) (2015).

[79] M. Singh, K. Nuutila, C. Kruse, A. Dermietzel, E. Caterson, E. Eriksson, Pixel grafting: an evolution of mincing for transplantation of full-thickness wounds, Plast. Reconstr. Surg. 137 (1) (2016) 92e–99e.

[80] F. Hackl, J. Bergmann, S.R. Granter, T. Koyama, E. Kiwanuka, B. Zuhaili, B. Pomahac, E.J. Caterson, J.P. Junker, E. Eriksson, Epidermal regeneration by micrograft transplantation with immediate 100-fold expansion, Plast. Reconstr. Surg. 129 (3) (2012) 443e–452e.

Supplementary Information:

In Vivo Printing of Growth Factor Eluting Adhesive Scaffolds Improves Wound Healing

Kristo Nuutila[1,†,*], Mohamadmahdi Samandari[2,†], Yori Endo[1], Yuteng Zhang[1], Jacob Quint[2,3], Tannin A. Schmidt[2], Ali Tamayol[2,3,*], Indranil Sinha[1,*]

[1] Division of Plastic Surgery, Brigham and Women's Hospital, Harvard Medical School, Boston, MA, 02115, USA

[2] Department of Biomedical Engineering, University of Connecticut, Farmington, CT 06030, USA

[3] Department of Mechanical and Materials Engineering, University of Nebraska-Lincoln, Lincoln, NE, 68588, USA

* Corresponding authors: isinha@bwh.harvard.edu (I. Sinha), atamayol@uchc.edu (A. Tamayol), kristo.nuutila@gmail.com (K. Nuutila)

[†] K. Nuutila and M. Samandari contributed equally to the work.

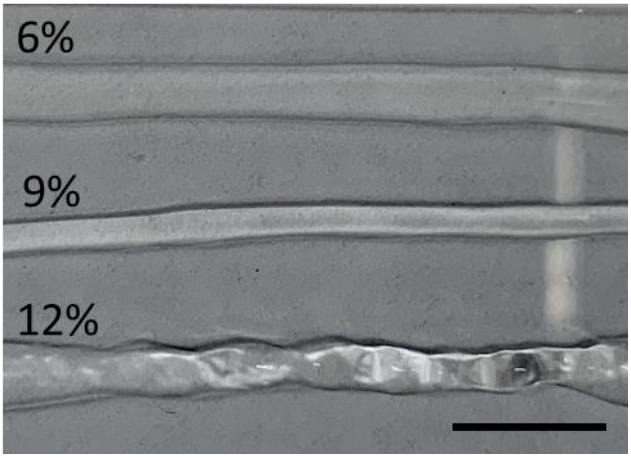

Figure S1. The printed filaments using different concentrations of the bioink. A 6% GelMA was not enough viscous to be compatible for our *in situ* printing strategy, while a 12% GelMA could rapidly become gel in room temperature and prevent formation of a smooth filament. A 9% GelMA was easily printable using our *in situ* printing strategy. Scale bar is 3 mm.

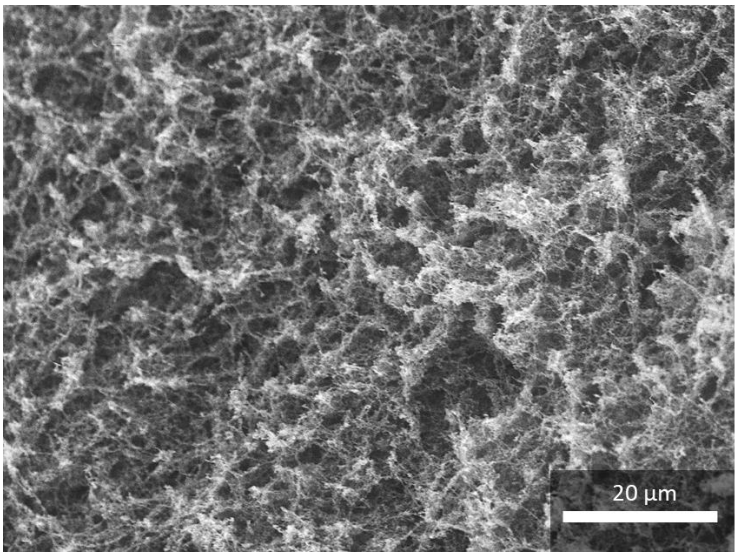

Figure S2. SEM analysis of the hydrogel internal structure upon critical point drying.

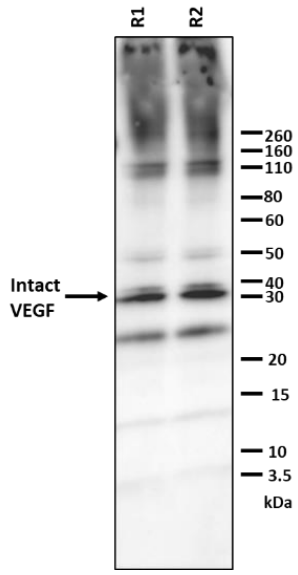

Figure S3. Western blot analysis of the VEGF sample collected on day 7 of the release study. The apparent molecular weight (~30 kDa) of the released VEGF from the hydrogel being consistent with the value provided by the manufacturer confirms that the majority of the protein remains intact after 7 days of incubation at 37°C. R1 and R2 shows duplicate samples from the release study.

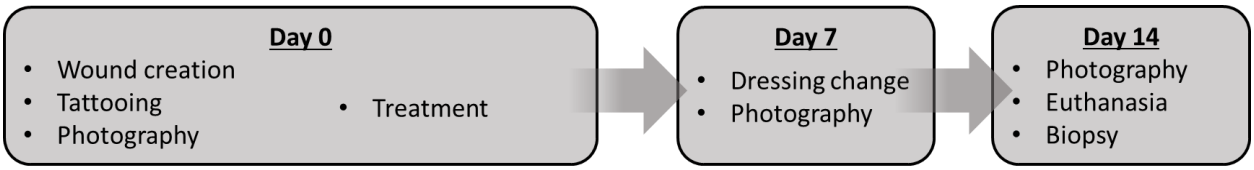

Figure S4. The workflow of animal studies in this work. At day 0, circular wounds were created on the dorsum of the pigs, followed by tattooing the wound border to track the contraction of the wounds. Photographs were taken, treatments were applied and wounds were covered with Tagederm dressings to prevent infection. On day 7, the dressing were removed, photographs were taken and new dressing were attached. Finally, on day 14, the dressings were removed, photographs were taken and animals were sacrificed. The tissues were harvested and fixed for analyses.

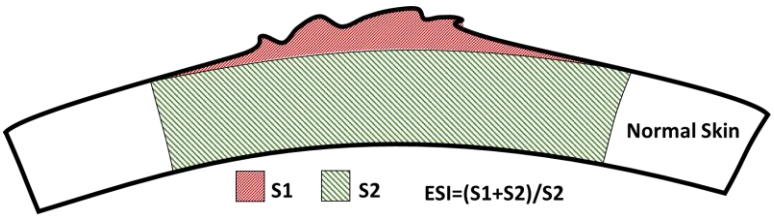

Figure S5. The measurement of the scar evaluation index (SEI) on day 14 post wound creation. The SEI is the ratio of total wound are tissue height (S1+S2) to the area of normal tissue below the elevated area due to scarring (S2).

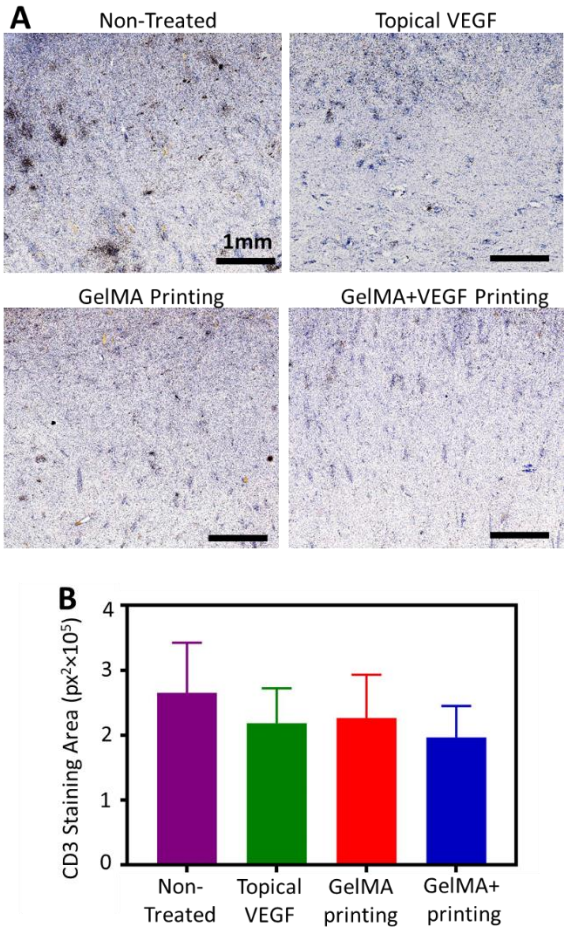

Figure S6. Immunohistological analysis of the wound bed to assess the level of immune response to the applied treatments on day 14 post surgery. The wound bed was examined for the expression of cluster of differentiation 3 (CD3), a protein highly expressed on the T-cells. (A) Representative images of wound bed immune cell infiltration in non-treated wounds compared to those treated with BPS containing VEGF administrated topically, *in vivo* printed blank GelMA (GelMA), and *in vivo* printed GelMA containing VEGF (GelMA+VEGF). The brown color indicates the presence of CD3. (B) Quantitative results of immune response to the various treatment methods applied in this work (n=6).